Supporting Information

A Tunable CT-State Rotaxane Gated by Solvent, Anions, and Aggregation

Wei-Liang Hu,[a,§] Yuan Yuan,[a,§] Gui-Yuan Wu,[a,*] Xian-Yi Zhang,[a] Wei-Jian Li,[b,*] Zhou Lu,[a,*]

[a] *Anhui Province Key Laboratory for Control and Applications of Optoelectronic Information Materials, School of Physics and Electronic Information, Anhui Normal University, Wuhu, 241002, China.*

[b] *School of Chemistry and Molecular Engineering, East China Normal University, Shanghai 200062, China.*

Correspondence:
Gui-Yuan Wu, Wei-Jian Li, Zhou Lu
wgy@ahnu.edu.cn (G-Y Wu); liweijian@ust.hk (W-J Li); zhoulu@ahnu.edu.cn (Z Lu);

Table of Contents

1. Materials and methods.

All solvents were dried according to standard procedures and all of them were degassed under N_2 for 30 minutes before use. All air-sensitive reactions were carried out under inert N_2 atmosphere. ^1H and ^{13}C NMR spectra were recorded on Bruker 500 MHz Spectrometer (^1H: 500 MHz; ^{13}C: 125 MHz) at 298 K. The ^1H and ^{13}C NMR chemical shifts are reported relative to the residual solvent signals. UV-Vis spectra were recorded in a quartz cell (light path 10 mm) on a Cary 50Bio UV-Visible spectrophotometer. Steady-state fluorescence spectra were recorded in a conventional quartz cell (light path 10 mm) on a Cary Eclipse fluorescence spectrophotometer. All the femtosecond transient absorption spectroscopy were acquired with a typical transmission pump-probe (UV/Vis pump-broadband supercontinuum probe) instrument. In this arrangement, a Ti: sapphaire regenerative amplifier (Spitfire Ace, Spectra Physics, Inc.) was employed to produce laser pulses (6 mJ, 1 kHz) with a pulse width of 80 fs and a center wavelength at 800 nm. The output laser was split into several laser beams, one of which was used to generate wavelength-tunable light serving as the pump laser for TAS via a downstream TOPAS instrument. The pump laser was further chopped with a 500 Hz mechanical chopper. Another laser beam propagated through an optical delay line (0-8 ns) and was then focused into a CaF_2 crystal to produce white light continuum, which serves as the probe light in the fs-TA. For the measurements, the solution samples were excited at 450 nm and then probe with a WLC pulse ranging from 350 to 700 nm. The instrument response function (IRF) of this system was determined to be ~120 fs under the same experimental conditions.

2. The stimuli responsiveness of [3]Rotaxane R.

Rotaxanes containing ureido groups, as a sophisticated molecular switch or prototype of molecular machines, can convert external ionic chemical signals into internal mechanical movements or functional state changes, demonstrating significant potential in the development of novel smart responsive materials (such as sensors, drug delivery carriers, molecular logic gates, etc.).[1-4] The introduction of ureido functional groups (-NH-CO-NH-) into rotaxane molecules endows them with remarkable ionic stimulus-responsive properties. This is mainly attributed to the unique structure of ureido groups: the hydrogen atoms on the two nitrogen atoms can act as excellent hydrogen bond donors, forming strong and specific multiple hydrogen bond interactions with specific anions (such as fluoride ions F^-, chloride ions Cl^-, acetate ions CH_3COO^-, dihydrogen phosphate ions $H_2PO_4^-$, etc.).

This anion recognition and binding behavior can be regarded as an effective chemical stimulus signal input. When the target anions complex with the ureido sites in the rotaxane, it significantly alters the local charge distribution, steric hindrance, and hydrogen bond network around the ureido groups. This perturbation of the local microenvironment effectively disrupts the non-covalent interaction balance (such as hydrogen bonds and van der Waals forces) between the components of the rotaxane (especially the macrocyclic host, such as calixarene, and the axle molecule, such as the ureido-containing dumbbell-shaped molecule). The direct consequence is the triggering of reversible and controlled displacement movements of the macrocyclic host along the axle molecule, thereby achieving the switching of the overall conformation or topological state of the rotaxane (such as the change in the interlocking degree between the quasi-rotaxane and rotaxane in [2]rotaxane). In this work, after the introduction of tetra-n-butylammonium acetate (TBAA), TBAA specifically complexes with the ureido sites in the rotaxane molecules. This complexation process triggers significant conformational changes within the rotaxane: the calixarene macrocyclic host, which was originally located near the ureido groups, moves towards the central core region along the central axis (typically a stilbene derivative, DSA) under the regulation of TBAA. This controlled displacement of the calixarene macrocyclic host directly alters its spatial relationship and electronic interaction with the central DSA core, thereby exerting a crucial influence on the relaxation dynamics of the excited state of the rotaxane molecule (particularly the excited state of the central DSA chromophore).

Scheme S1. Cartoon representation of the anion-induced motions of the DEP[5]A macrocycles in [3]rotaxane R.

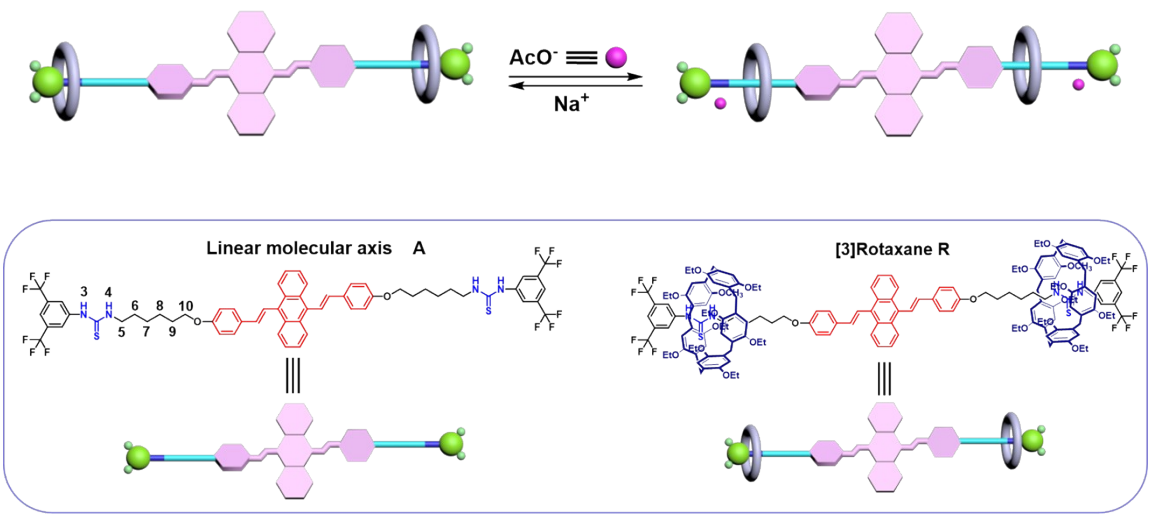

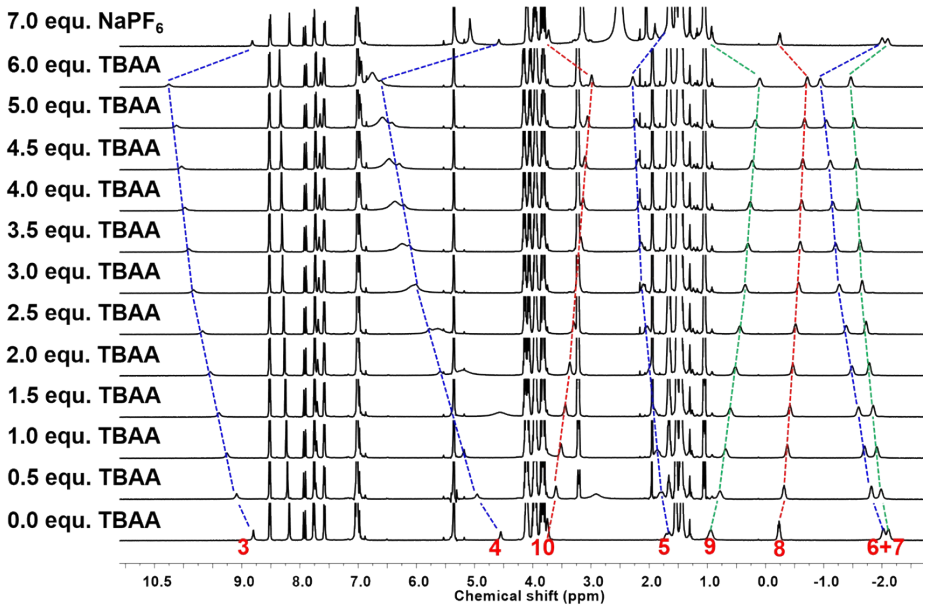

Figure S1. ^{1}H NMR spectra (CD_2Cl_2, 298 K, 500 MHz) (bottom) of the anion-induced motions of the DEP[5]A macrocycles in [3]rotaxane R.

3. The steady-state absorption and fluorescence emission spectra.

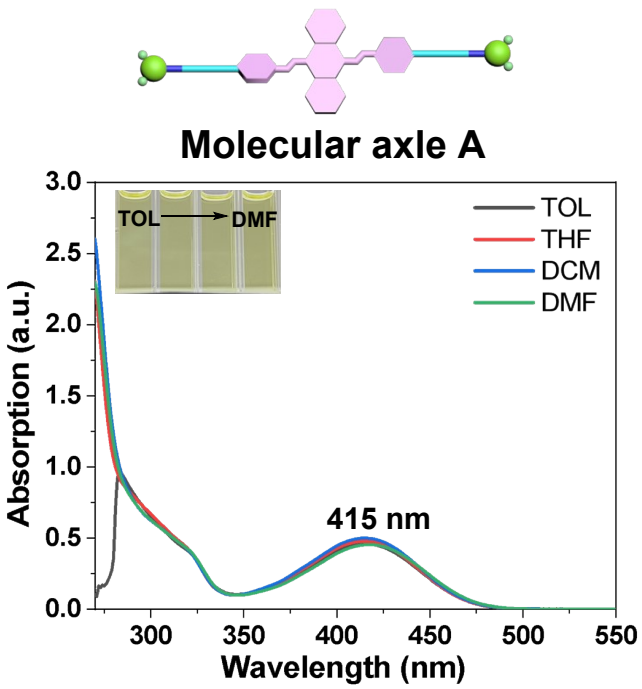

Figure S2. The steady-state absorption spectra of the axle **A** in TOL, THF, DCM and DMF solutions (c = 30 μM).

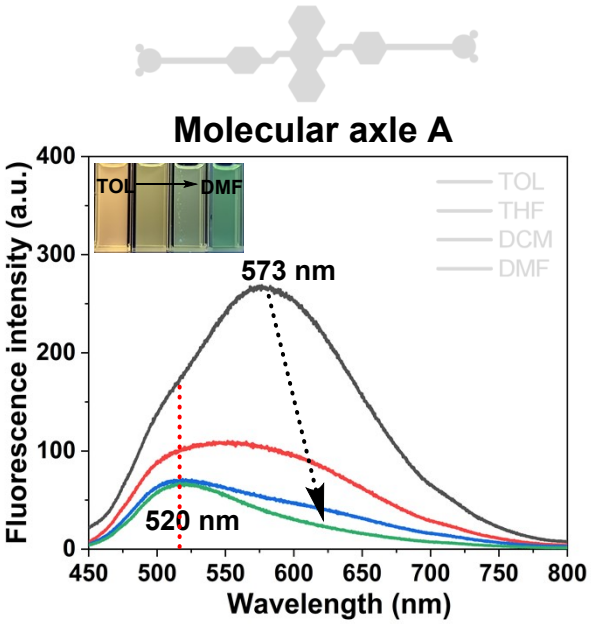

Figure S3. The fluorescence emission spectra of the axle **A** in TOL, THF, DCM and DMF solutions (c = 30 μM, λex= 400 nm).

Table S1. Photophysical data of axle **A**, [3]rotaxane **R** and [3]rotaxane **R**+TBAA.

	Solvents	λabs,max/nm	λem,max/nm	τ_F/ns	Φ/%
Axle **A**	TOL	415	520, 573	1.01	1.2
	THF	415	520, 600	0.48	0.55
	DCM	415	520, 625	0.33	0.21
	DMF	420	520	0.16	0.10
[3]Rotaxane **R**	TOL	295, 415	530, 628	2.1	17.8
	THF	295, 415	530, 650	0.72	1.4
	DCM	295, 415	530, 675	0.41	0.35
	DMF	295, 420	539	0.22	0.12
[3]Rotaxane **R** + TBAA	TOL	295, 415	525, 575	1.5	5.3
	THF	295, 415	525, 600	0.55	0.68
	DCM	295, 415	525, 620	0.48	0.3
	DMF	295, 420	525	0.2	0.12

5

Table S2. Radiative and non-radiative rates of alxe **A**, [3]rotaxane **R** and [3]rotaxane **R**+TBAA. (τ_F, fluorescence lifetime. k_r, radiation rate. k_{nr}, non-radiation rate.)

$$k_r = \Phi/\tau_F \qquad k_{nr} = (1-\Phi)/\tau_F$$

	Axle **A**		[3]Rotaxane **R**		[3]Rotaxane **R** + TBAA	
Solvents	k_r (s^{-1})	k_{nr} (s^{-1})	k_r (s^{-1})	k_{nr} (s^{-1})	k_r (s^{-1})	k_{nr} (s^{-1})
TOL	1.19×10^7	0.98×10^9	8.48×10^7	0.39×10^9	3.53×10^7	0.63×10^9
THF	1.15×10^7	2.07×10^9	1.94×10^7	1.37×10^9	1.24×10^7	1.81×10^9
DCM	0.64×10^7	3.02×10^9	0.85×10^7	2.43×10^9	0.63×10^7	2.00×10^9
DMF	0.62×10^7	6.24×10^9	0.59×10^7	4.54×10^9	0.6×10^7	4.99×10^9

Table S3. Photophysical data of rotaxane aggregates solutions.

	λabs,max/nm	λem,max/nm	τ_F/ns	Φ/%
0% hexane	295, 414	682	0.41	0.35
5% hexane	295, 415	680	0.45	0.4
10% hexane	295, 415	676	0.5	0.45
20% hexane	295, 416	670	0.52	0.56
40% hexane	295, 416	665	1.51	5.66
70% hexane	295, 417	650	1.62	15.7
90% hexane	295, 417	635	3.21	47.3
95% hexane	295, 418	625	3.98	51.8

Table S4. Radiative and non-radiative rates of rotaxane aggregate solutions.

	0%	5%	10%	20%	40%	70%	90%	95%
kr (s^{-1})	0.85×10^7	0.89×10^7	0.9×10^7	1.08×10^7	3.74×10^7	9.69×10^7	14.7×10^7	14.01×10^7

*k*nr (s^{-1})	24.3×10^8	22.1×10^8	19.9×10^8	19.1×10^8	6.25×10^8	5.2×10^8	1.64×10^8	1.21×10^8

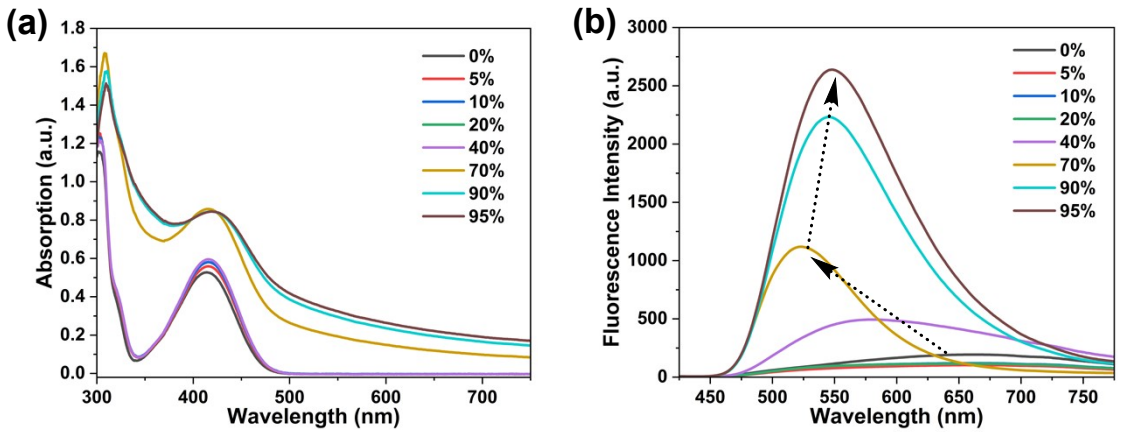

Figure S4. The steady-state absorption (a) and fluorescence emission (b) spectra of the [3]rotaxane R-aggregates in H_2O/THF mixtures with different H_2O contents (c = 30 μM, V_{H2O}/V_{mix}: 0%, 5%, 10%, 5 20%, 40%, 70%, 90%, 95%) (λ_{ex}= 400 nm).

4. Femtosecond transient absorption (fs-TA) spectra.

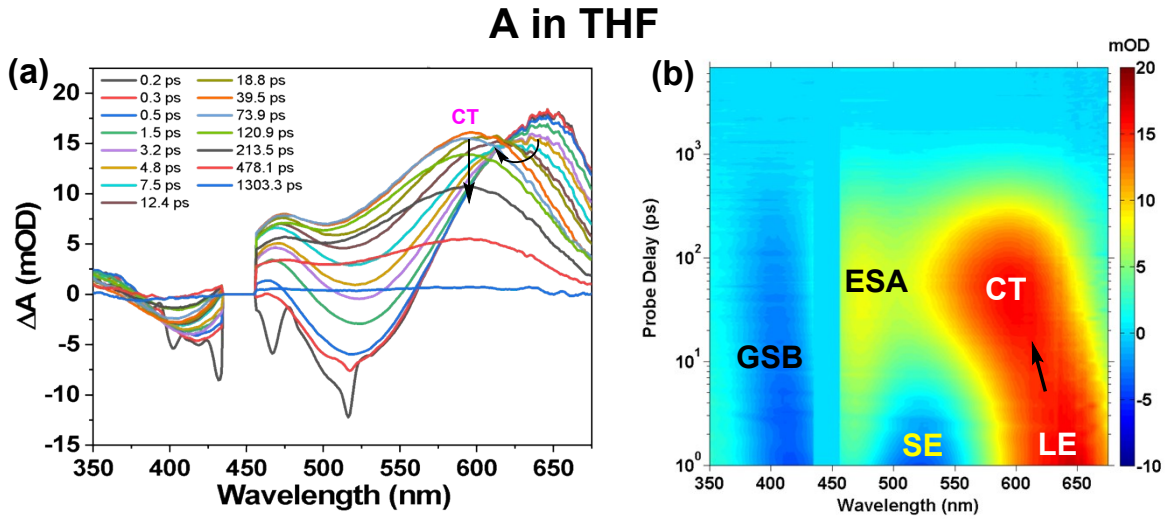

Figure S5. The fs-TA spectra (a) and TA maps (b) of linear molecular axle **A** in THF (30 μM, λex =

450 nm).

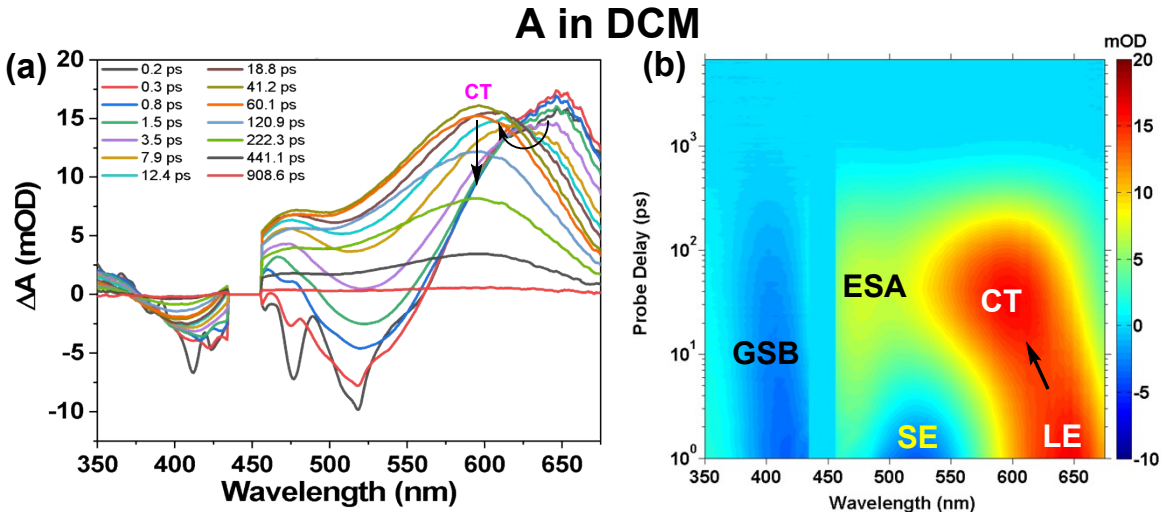

Figure S6. The fs-TA spectra (a) and TA maps (b) of linear molecular axle **A** in DCM (30 μM, λex = 5 450 nm).

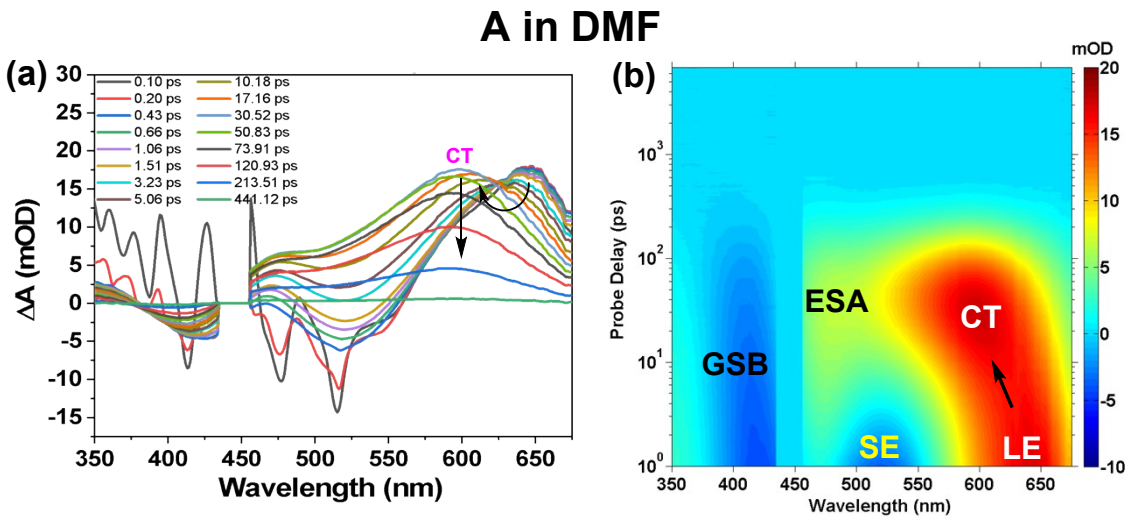

Figure S7. The fs-TA spectra (a) and TA maps (b) of linear molecular axle **A** in DMF (30 μM, λex = 450 nm).

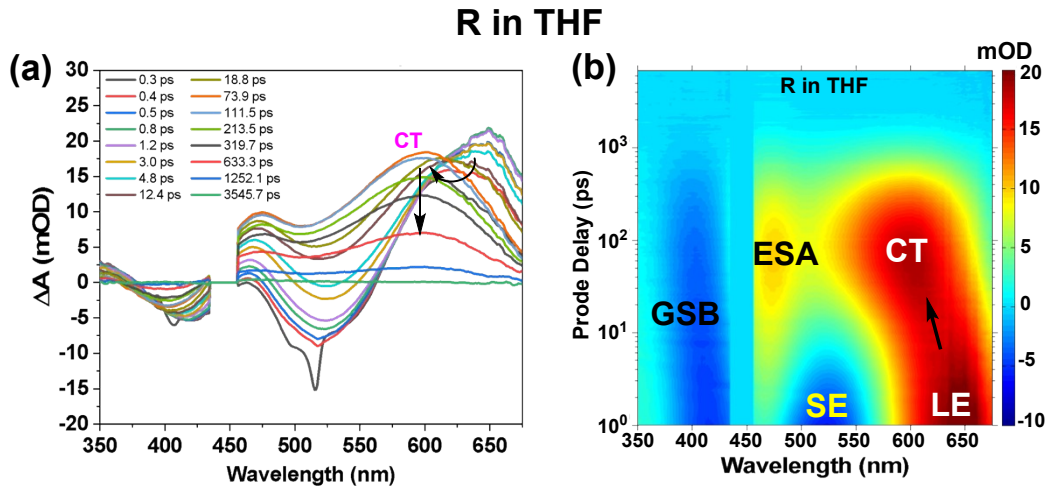

Figure S8. The fs-TA spectra (a) and TA maps (b) of rotaxane **R** in THF (30 μM, λex = 450 nm).

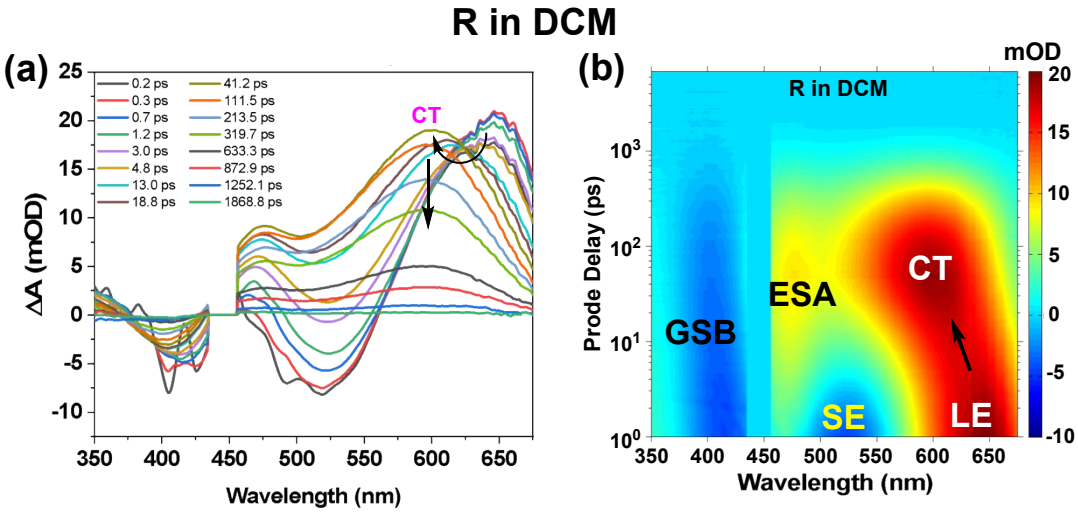

Figure S9. The fs-TA spectra (a) and TA maps (b) of rotaxane R in DCM (30 μM, λex = 450 nm).

5

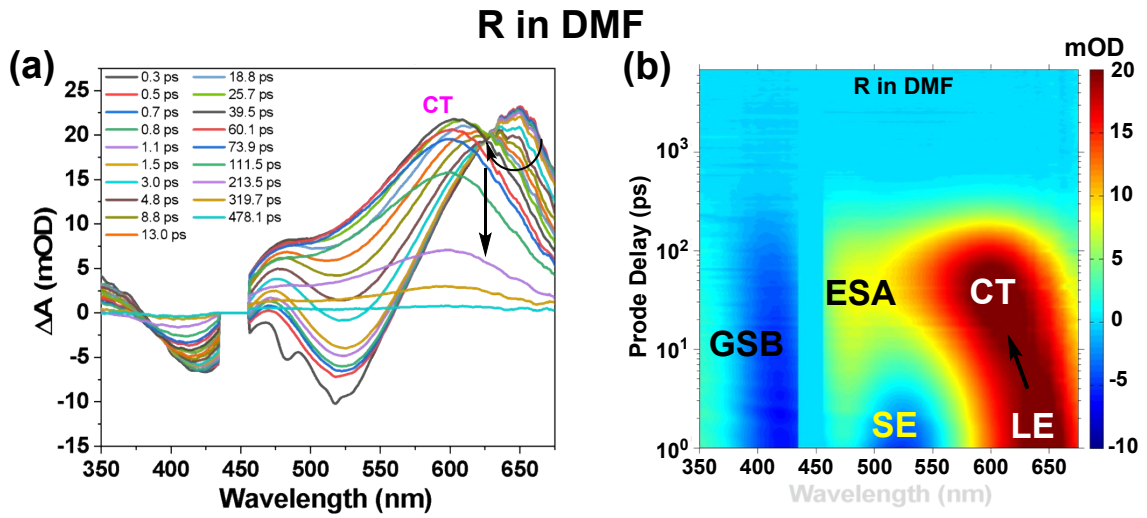

Figure S10. The fs-TA spectra (a) and TA maps (b) of rotaxane **R** in DMF (30 μM, λex = 450 nm).

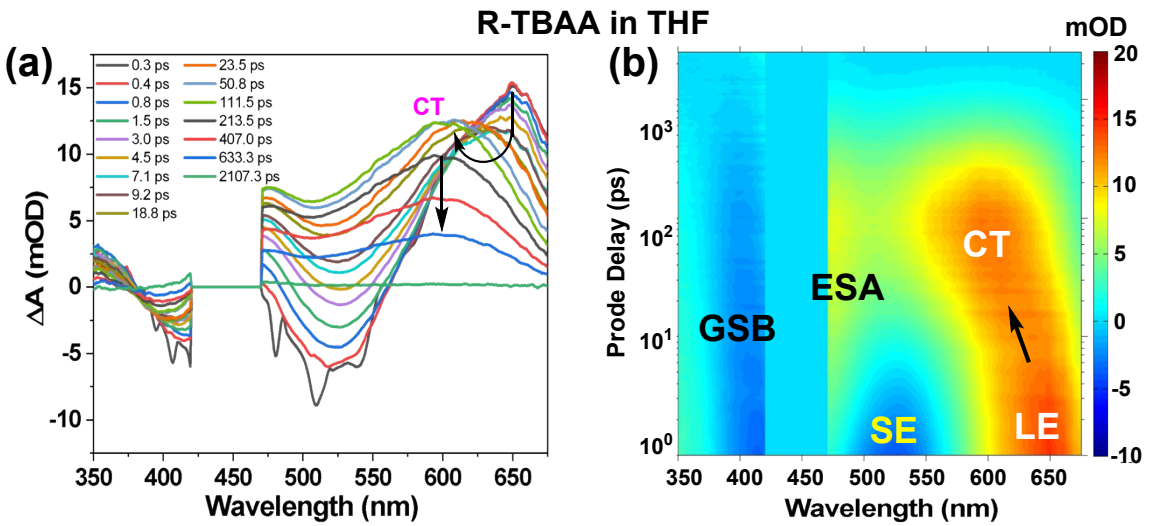

5 Figure S11. The fs-TA spectra (a) and TA maps (b) of rotaxane **R**+TBAA in THF (30 μM, λex = 450 nm).

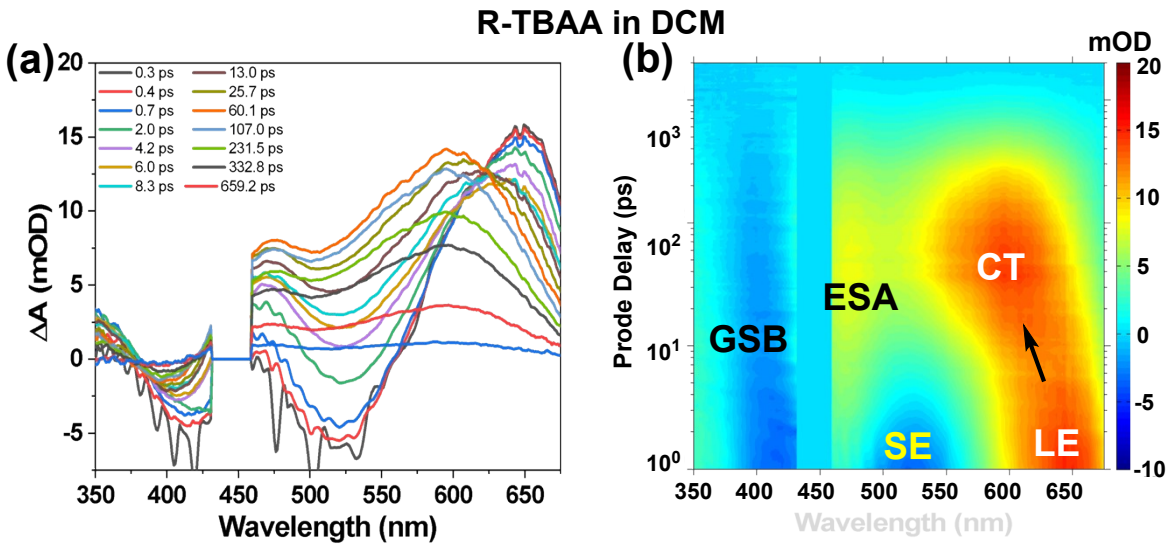

Figure S12. The fs-TA spectra (a) and TA maps (b) of rotaxane **R**+TBAA in DCM (30 μM, λex = 450 nm).

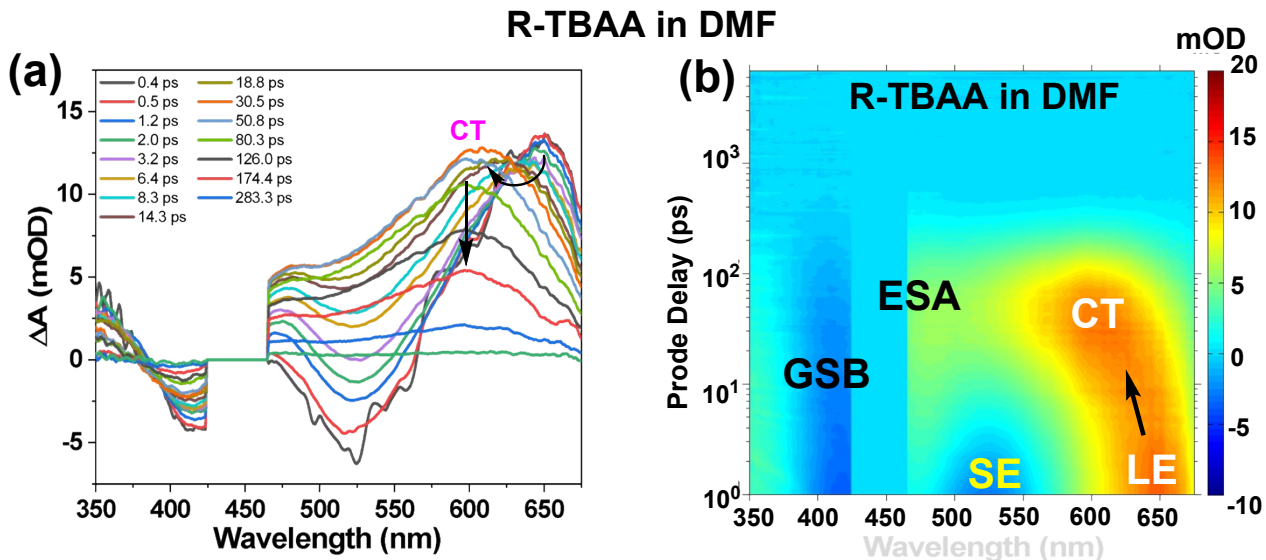

5 Figure S13. The fs-TA spectra (a) and TA maps (b) of rotaxane **R**+TBAA in DMF (30 μM, λex = 450 nm).

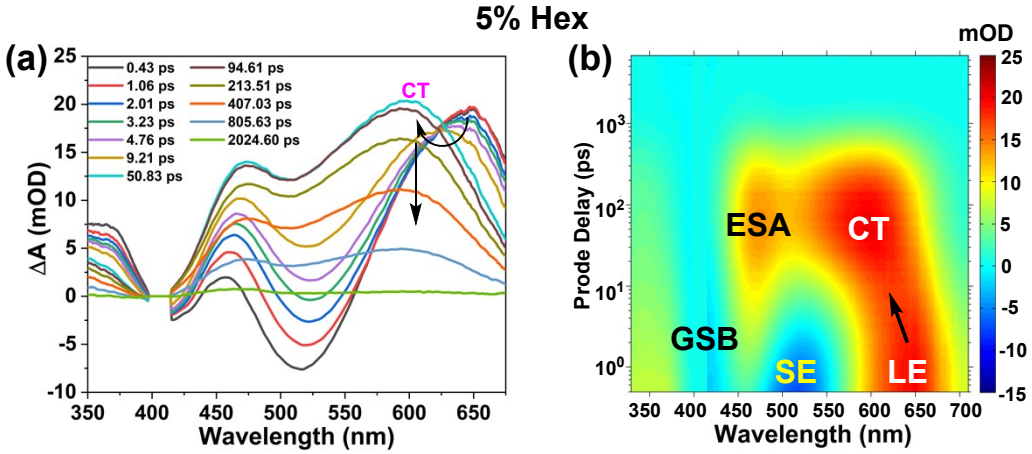

Figure S14. The fs-TA spectra (a) and TA maps (b) of [3]rotaxane in mixed solvents of DCM and n-hexane (V_{Hex}/V_{mix} = 5/100) (c = 30 μM).

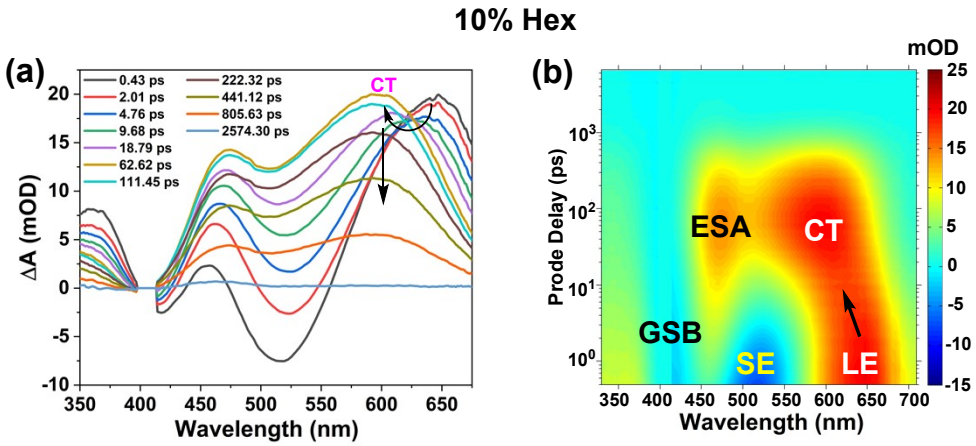

5 Figure S15. The fs-TA spectra (a) and TA maps (b) of [3]rotaxane in mixed solvents of DCM and n-hexane (V_{Hex}/V_{mix} = 10/100) (c = 30 μM).

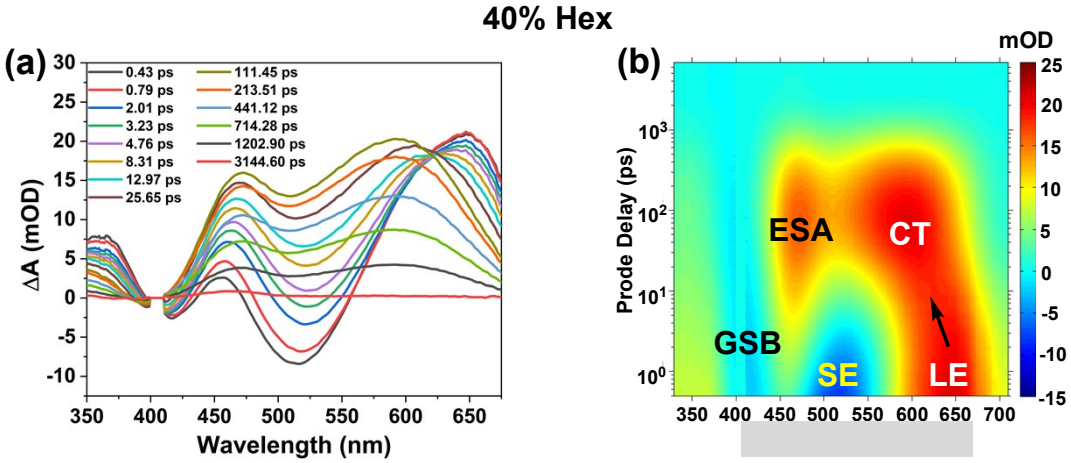

Figure S16. The fs-TA spectra (a) and TA maps (b) of [3]rotaxane in mixed solvents of dichloromethane and n-hexane (V_{Hex}/V_{mix} = 40/100) (c = 30 μM).

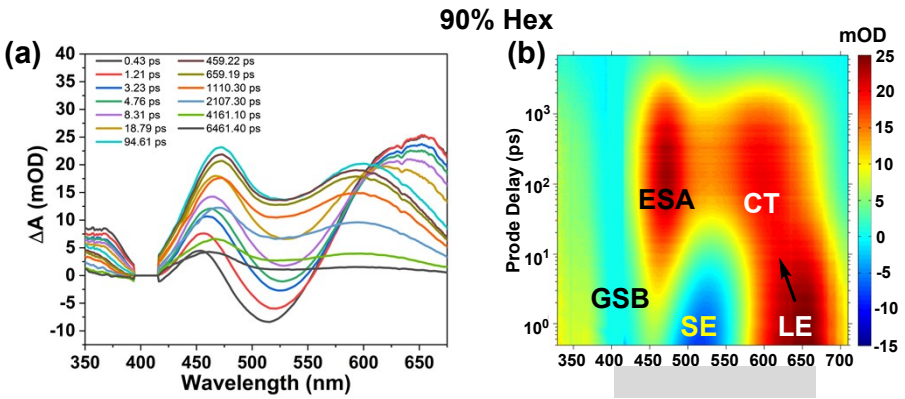

Figure S17. The fs-TA spectra (a) and TA maps (b) of [3]rotaxane in mixed solvents of dichloromethane and n-hexane (V_{Hex}/V_{mix} = 90/100) (c = 30 μM).

5. Global fitting based on the analysis of the fs-TA measurements.

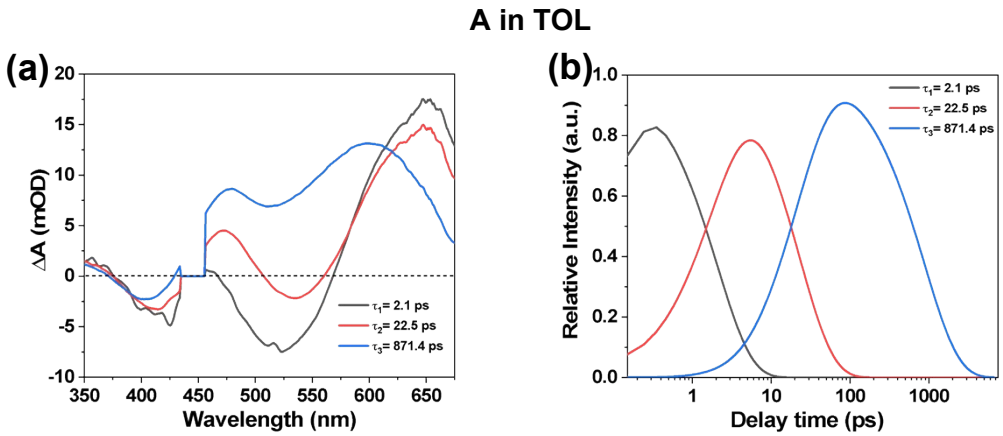

Figure S18. Species-associated different spectra (SADS) (a) and corresponding concentration evolution kinetics (b) of transient species obtained from the global analyses of fs-TA spectra for **A** in TOL.

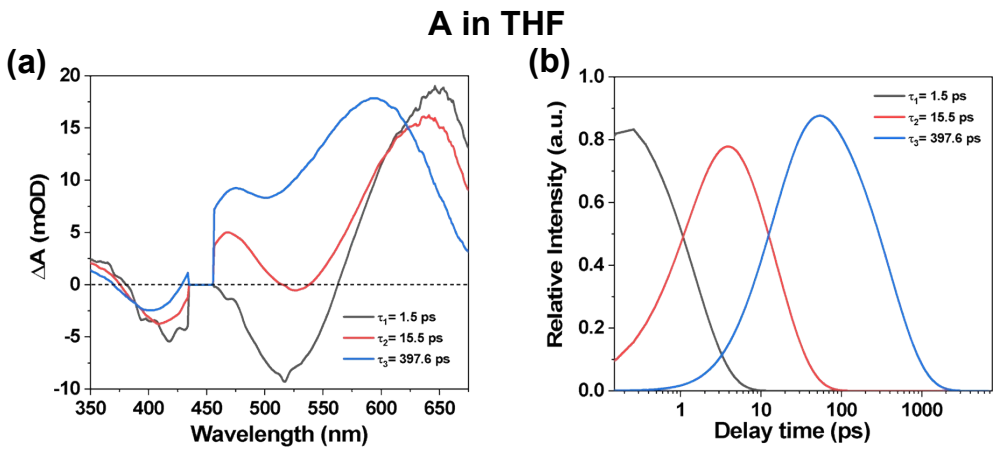

Figure S19. Species-associated different spectra (SADS) (a) and corresponding concentration evolution kinetics (b) of transient species obtained from the global analyses of fs-TA spectra for **A** in THF.

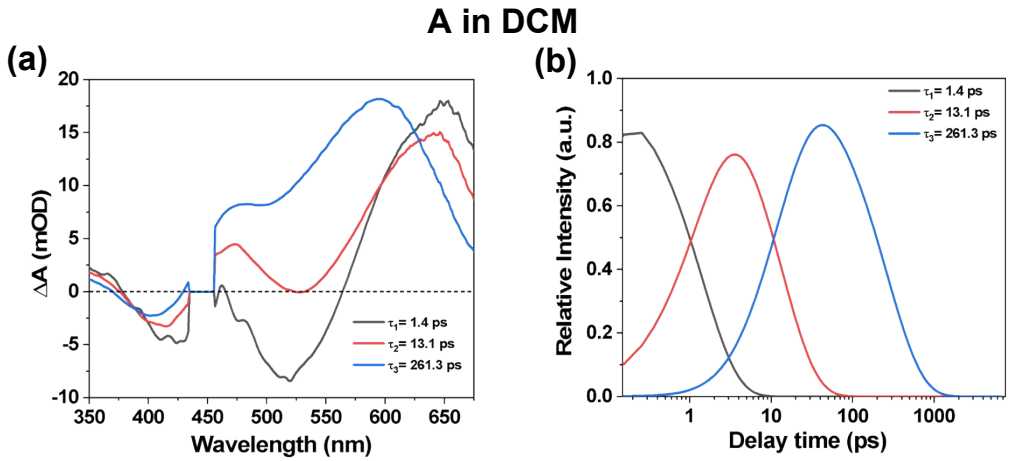

Figure S20. Species-associated different spectra (SADS) (a) and corresponding concentration evolution kinetics (b) of transient species obtained from the global analyses of fs-TA spectra for **A** in DCM.

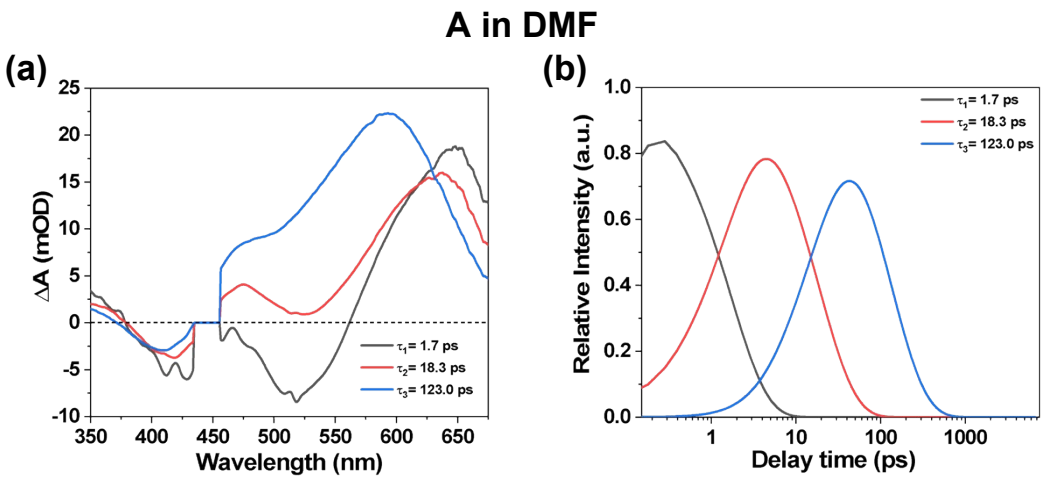

Figure S21. Species-associated different spectra (SADS) (a) and corresponding concentration evolution kinetics (b) of transient species obtained from the global analyses of fs-TA spectra for **A** in DMF.

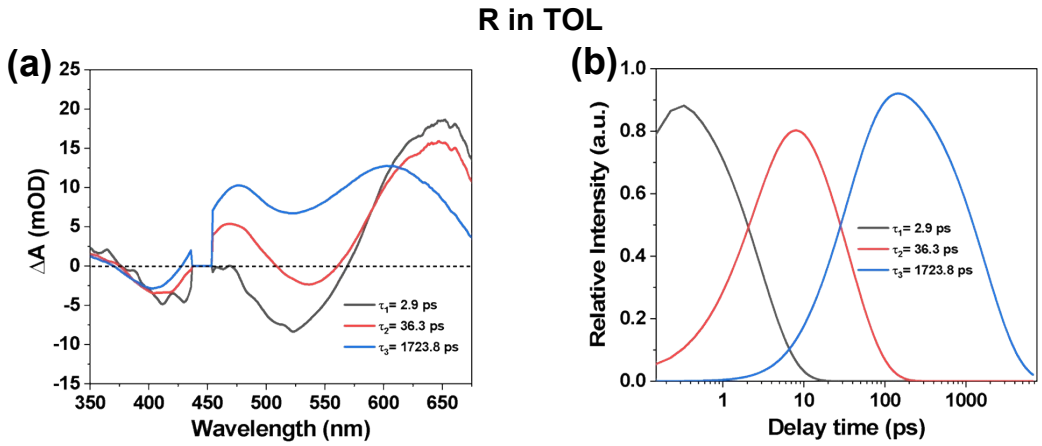

Figure S22. Species-associated different spectra (SADS) (a) and corresponding concentration evolution kinetics (b) of transient species obtained from the global analyses of fs-TA spectra for **R** in TOL.

5

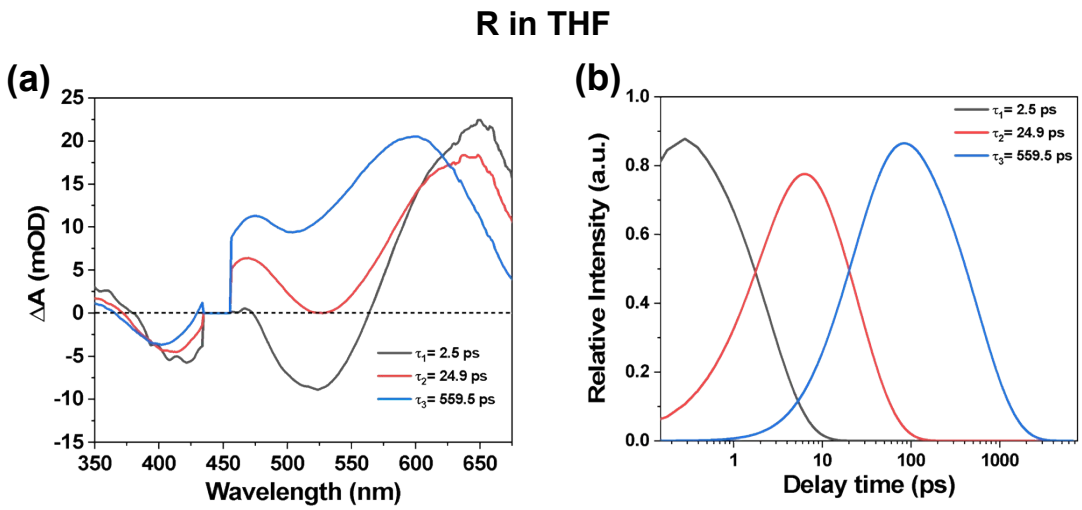

Figure S23. Species-associated different spectra (SADS) (a) and corresponding concentration evolution kinetics (b) of transient species obtained from the global analyses of fs-TA spectra for **R** in THF.

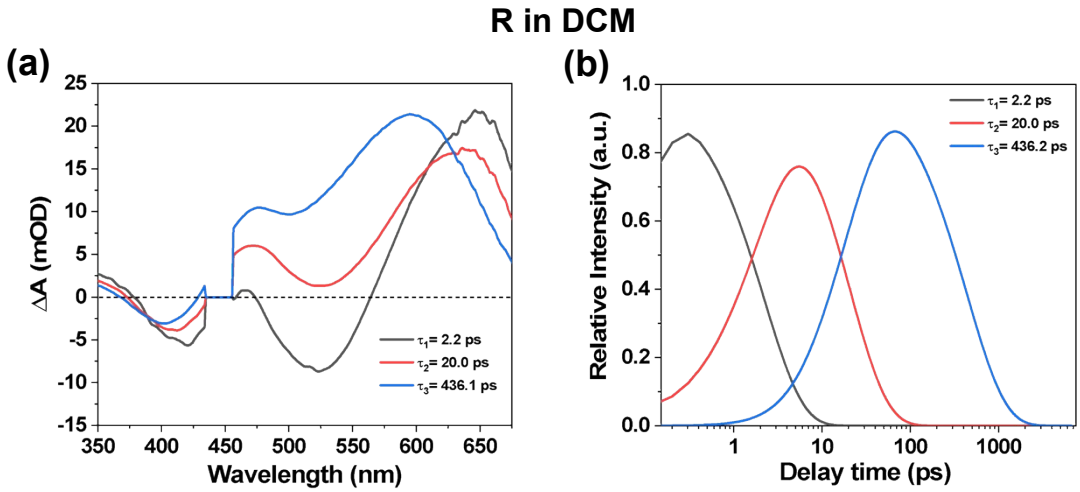

Figure S24. Species-associated different spectra (SADS) (a) and corresponding concentration evolution kinetics (b) of transient species obtained from the global analyses of fs-TA spectra for **R** in DCM.

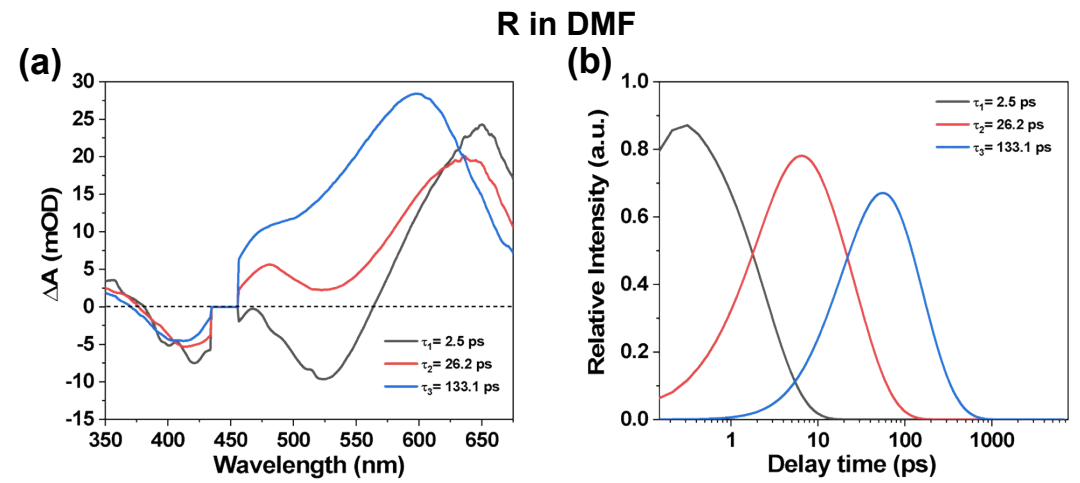

Figure S25. Species-associated different spectra (SADS) (a) and corresponding concentration evolution kinetics (b) of transient species obtained from the global analyses of fs-TA spectra for **R** in DMF.

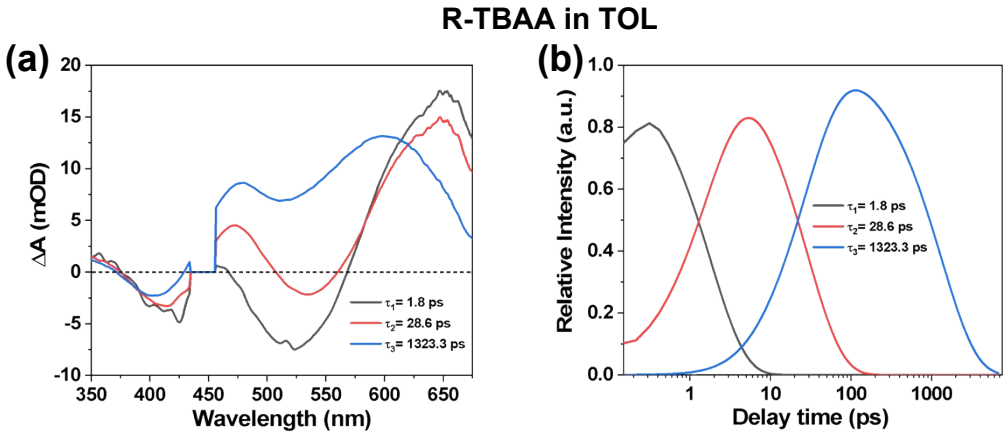

Figure S26. Species-associated different spectra (SADS) (a) and corresponding concentration evolution kinetics (b) of transient species obtained from the global analyses of fs-TA spectra for **R**-TBAA in TOL.

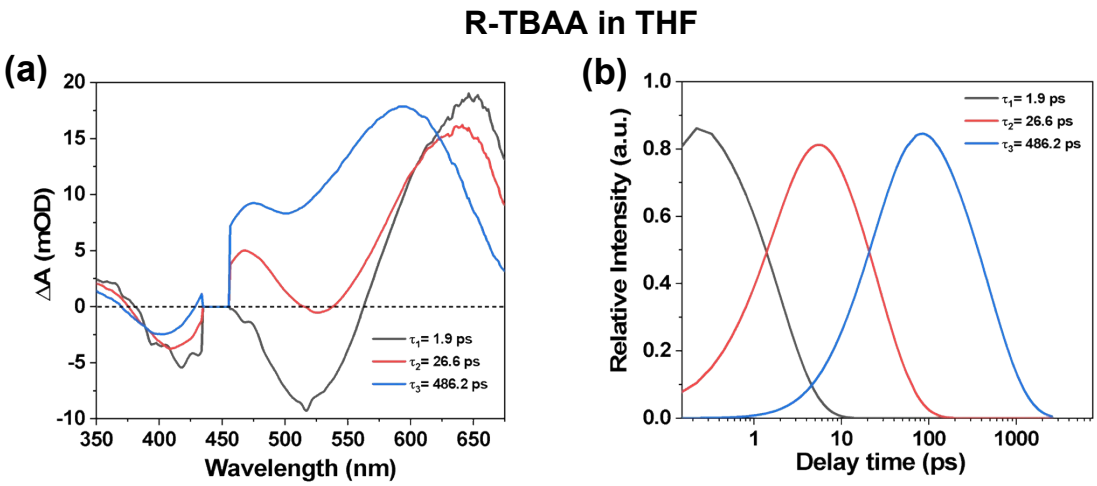

Figure S27. Species-associated different spectra (SADS) (a) and corresponding concentration evolution kinetics (b) of transient species obtained from the global analyses of fs-TA spectra for **R**-TBAA in THF.

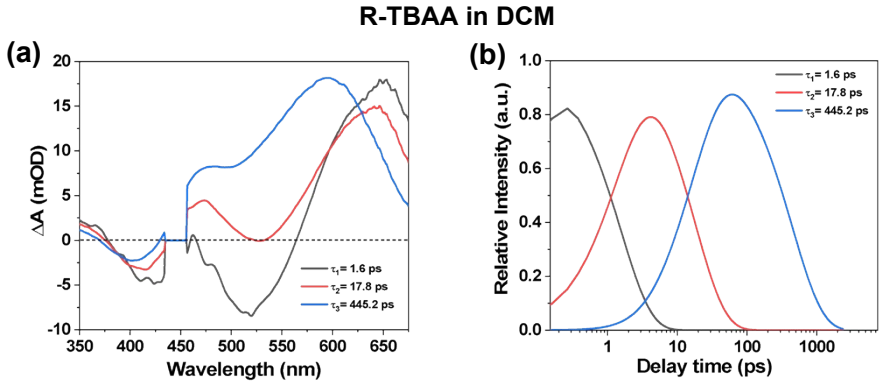

Figure S28. Species-associated different spectra (SADS) (a) and corresponding concentration evolution kinetics (b) of transient species obtained from the global analyses of fs-TA spectra for **R**-TBAA in DCM.

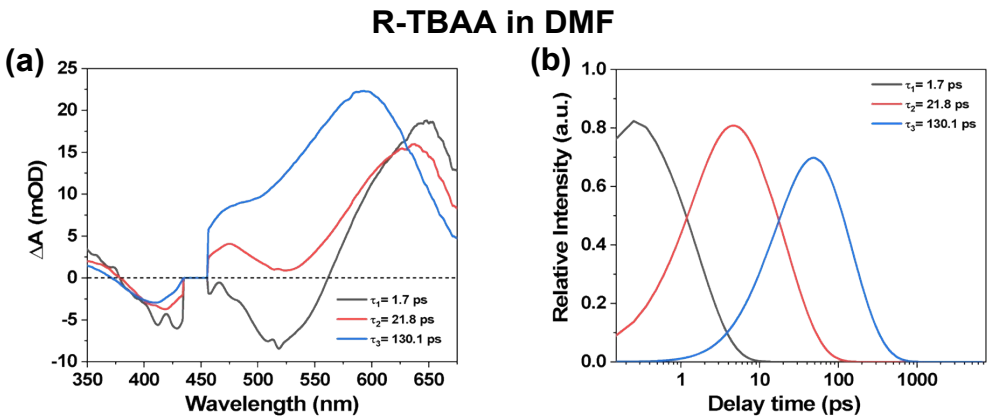

5

Figure S29. Species-associated different spectra (SADS) (a) and corresponding concentration evolution kinetics (b) of transient species obtained from the global analyses of fs-TA spectra for **R**-TBAA in DMF.

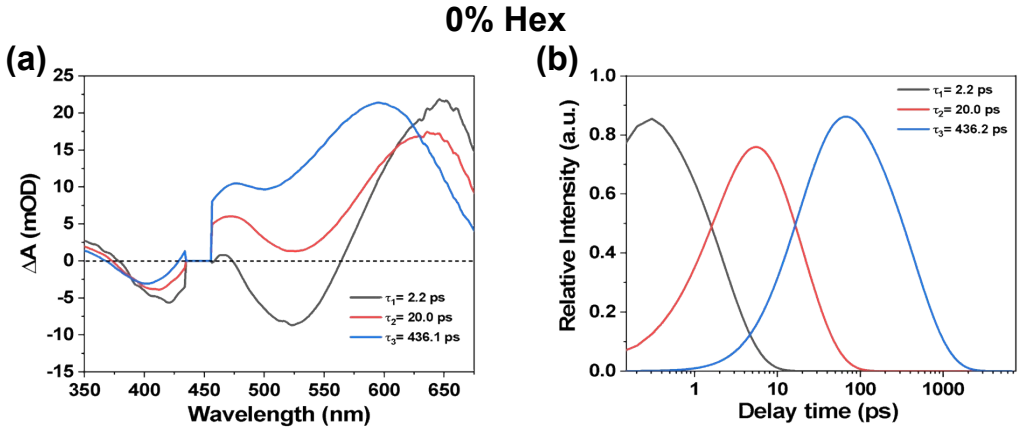

Figure S30. Species-associated different spectra (SADS) (a) and corresponding concentration evolution kinetics (b) of transient species obtained from the global analyses of fs-TA spectra for [3]rotaxane in mixed solvents of DCM and n-hexane (c = 30 μM, V_{hexane}/V_{mix} = 0%).

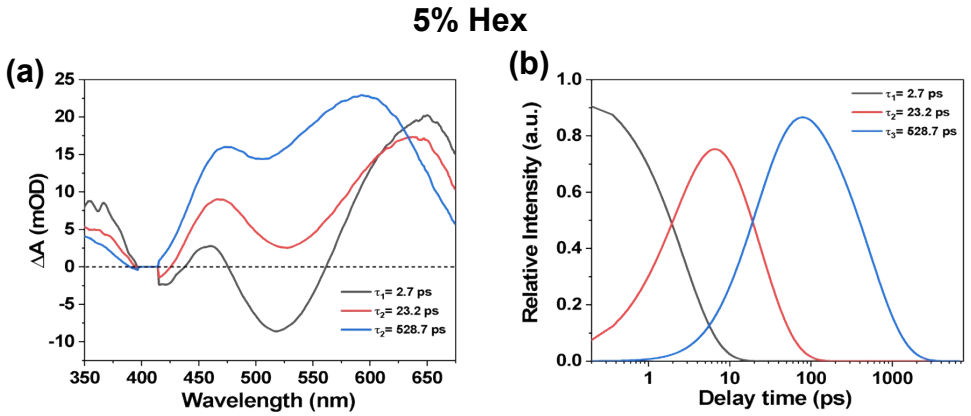

Figure S31. Species-associated different spectra (SADS) (a) and corresponding concentration evolution kinetics (b) of transient species obtained from the global analyses of fs-TA spectra for [3]rotaxane in mixed solvents of DCM and n-hexane (c = 30 μM, V_{hexane}/V_{mix} = 5%).

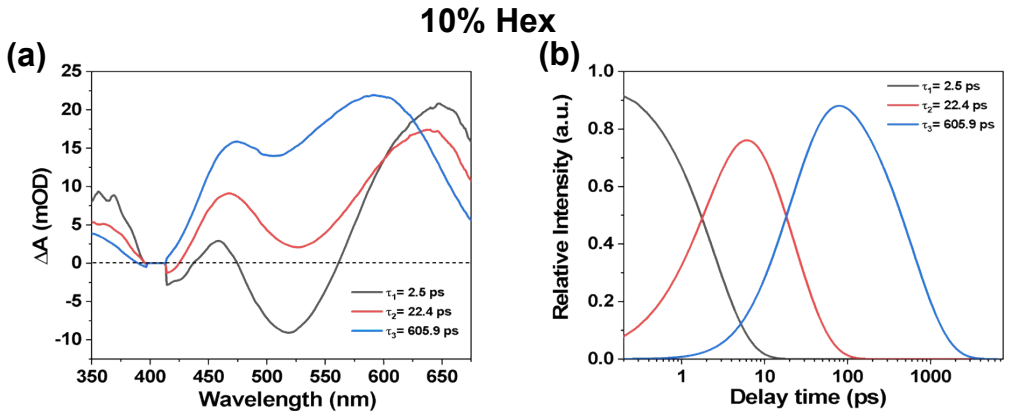

Figure S32. Species-associated different spectra (SADS) (a) and corresponding concentration evolution kinetics (b) of transient species obtained from the global analyses of fs-TA spectra for [3]rotaxane in mixed solvents of DCM and n-hexane (c = 30 μM, V_{hexane}/V_{mix} = 10%).

5

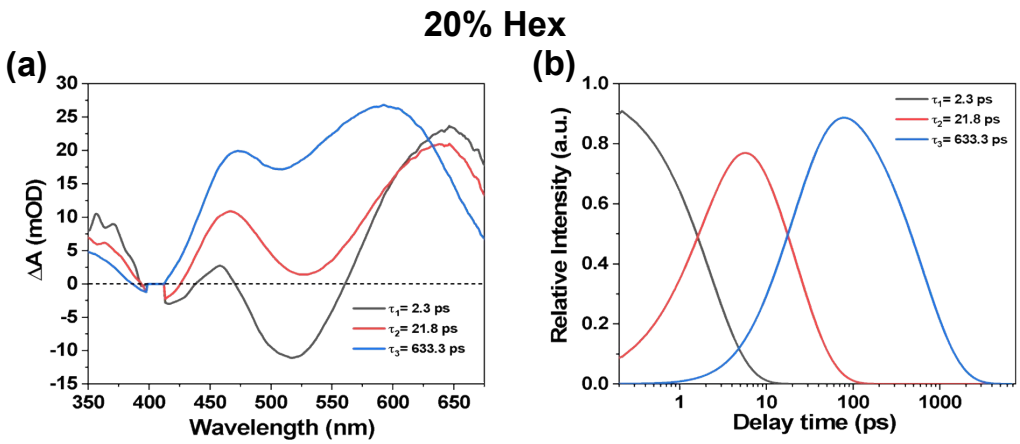

Figure S33. Species-associated different spectra (SADS) (a) and corresponding concentration evolution kinetics (b) of transient species obtained from the global analyses of fs-TA spectra for [3]rotaxane in mixed solvents of DCM and n-hexane (c = 30 μM, V_{hexane}/V_{mix} = 20%).

10

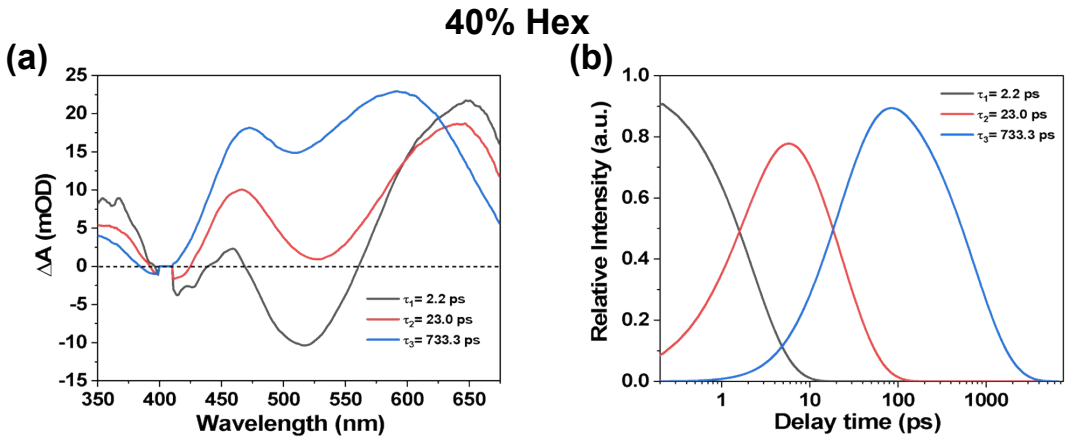

Figure S34. Species-associated different spectra (SADS) (a) and corresponding concentration evolution kinetics (b) of transient species obtained from the global analyses of fs-TA spectra for [3]rotaxane in mixed solvents of DCM and n-hexane (c = 30 μM, V_{hexane}/V_{mix} = 40%).

5

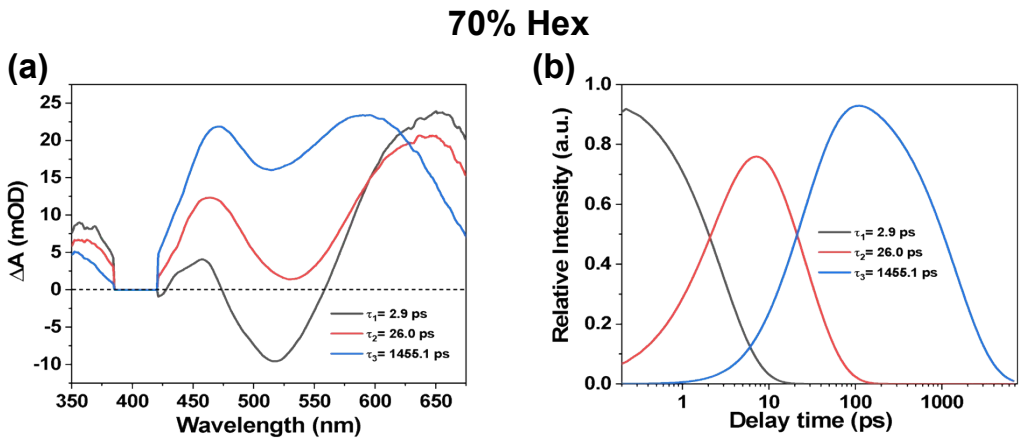

Figure S35. Species-associated different spectra (SADS) (a) and corresponding concentration evolution kinetics (b) of transient species obtained from the global analyses of fs-TA spectra for [3]rotaxane in mixed solvents of DCM and n-hexane (c = 30 μM, V_{hexane}/V_{mix} = 70%).

10

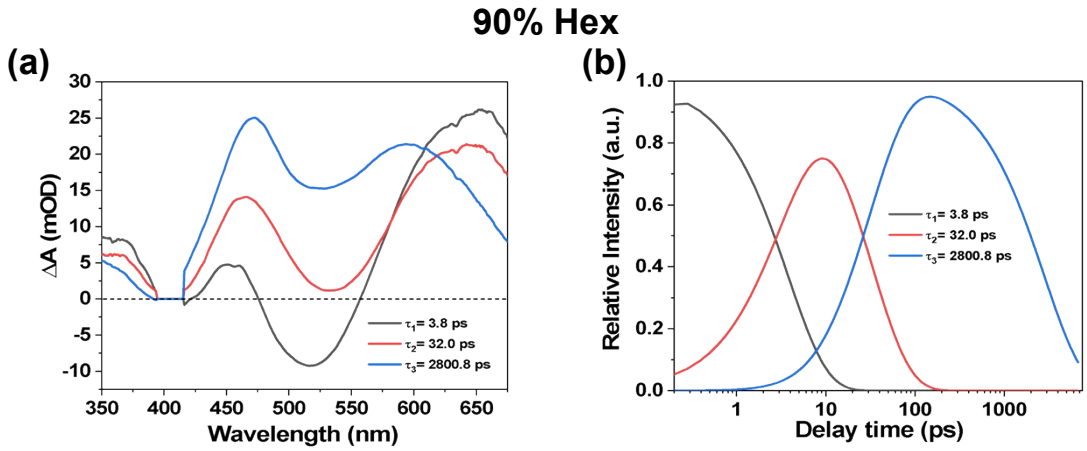

Figure S36. Species-associated different spectra (SADS) (a) and corresponding concentration evolution kinetics (b) of transient species obtained from the global analyses of fs-TA spectra for [3]rotaxane in mixed solvents of DCM and n-hexane (c = 30 μM, V_{hexane}/V_{mix} = 90%).

5

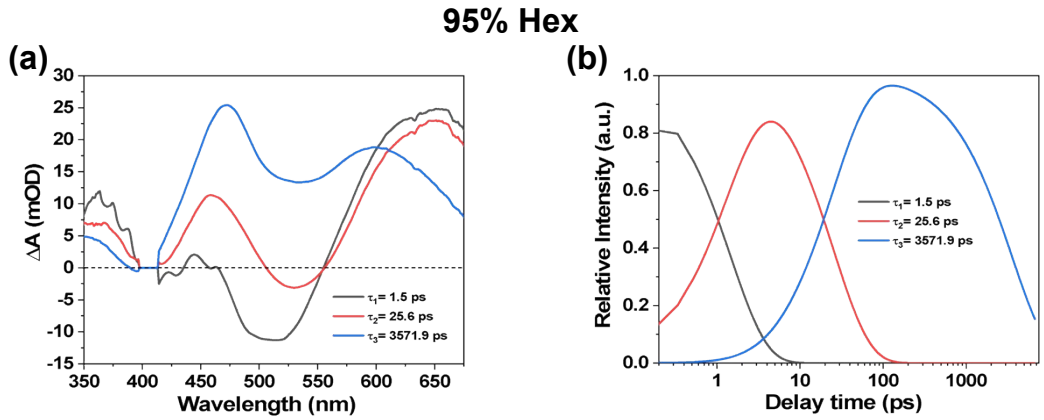

Figure S37. Species-associated different spectra (SADS) (a) and corresponding concentration evolution kinetics (b) of transient species obtained from the global analyses of fs-TA spectra for [3]rotaxane in mixed solvents of DCM and n-hexane (c = 30 μM, V_{hexane}/V_{mix} = 95%).

10

6. ^{1}H NMR and ^{13}C NMR spectra of [3]rotaxane R and linear molecular axle A.

[3]Rotaxane R: ^{1}H NMR (500 MHz, CD_2Cl_2) δ 8.77 (s, 2H), 8.49 (dd, J = 6.8, 3.3 Hz, 4H), 8.15 (s, 4H), 7.89 (d, J = 16.4 Hz, 2H), 7.73 (d, J = 8.6 Hz, 6H), 7.55 (dd, J = 6.9, 3.1 Hz, 4H), 6.99 (t, J = 6.0 Hz, 26H), 4.52 (s, 2H), 4.08 (ddd, J = 10.9, 7.9, 3.3 Hz, 20H), 3.98 – 3.90 (m, 20H), 3.78 (dt, J = 33.8, 16.9 Hz, 24H), 1.65 (s, 4H), 1.51 (t, J = 6.9 Hz, 30H), 1.41 (t, J = 6.8 Hz, 30H), 0.90 (s, 4H), -0.26 (s, 4H), -2.09 (d, J = 42.1 Hz, 8H). ^{13}C NMR (125 MHz, CD_2Cl_2) δ 180.07, 159.65, 150.19, 149.38, 141.64, 136.98, 132.87, 131.71, 131.44, 131.18, 130.91, 130.04, 129.73, 129.45, 128.53, 127.88, 126.62, 125.19 (s), 124.37, 122.77, 122.38, 117.56, 115.17, 114.52, 114.33, 113.95, 69.41, 65.00, 63.52, 45.26, 29.55, 29.15, 28.23, 25.88, 24.90, 23.13, 15.42, 15.30.

Linear molecular axis A: ^{1}H NMR (500 MHz, CD_2Cl_2) δ 8.41 (dd, J = 6.7, 3.3 Hz, 4H), 7.81 (dd, J = 37.9, 21.4 Hz, 8H), 7.63 (d, J = 8.7 Hz, 4H), 7.55 (s, 2H), 7.48 (dd, J = 6.8, 3.3 Hz, 4H), 6.99 (d, J = 8.7 Hz, 4H), 6.87 (d, J = 16.4 Hz, 2H), 6.14 (s, 1H), 4.05 (t, J = 6.4 Hz, 4H), 3.64 (s, 4H), 1.89 – 1.80 (m, 4H), 1.75 – 1.68 (m, 4H), 1.57 (s, 5H), 1.48 (s, 4H). ^{13}C NMR (125 MHz, CD_2Cl_2) δ 184.67, 162.67, 145.42, 140.38, 136.07, 133.26, 132.91, 131.23, 129.69, 128.49, 127.88, 125.68, 118.07, 71.01, 47.53, 29.83, 28.94.

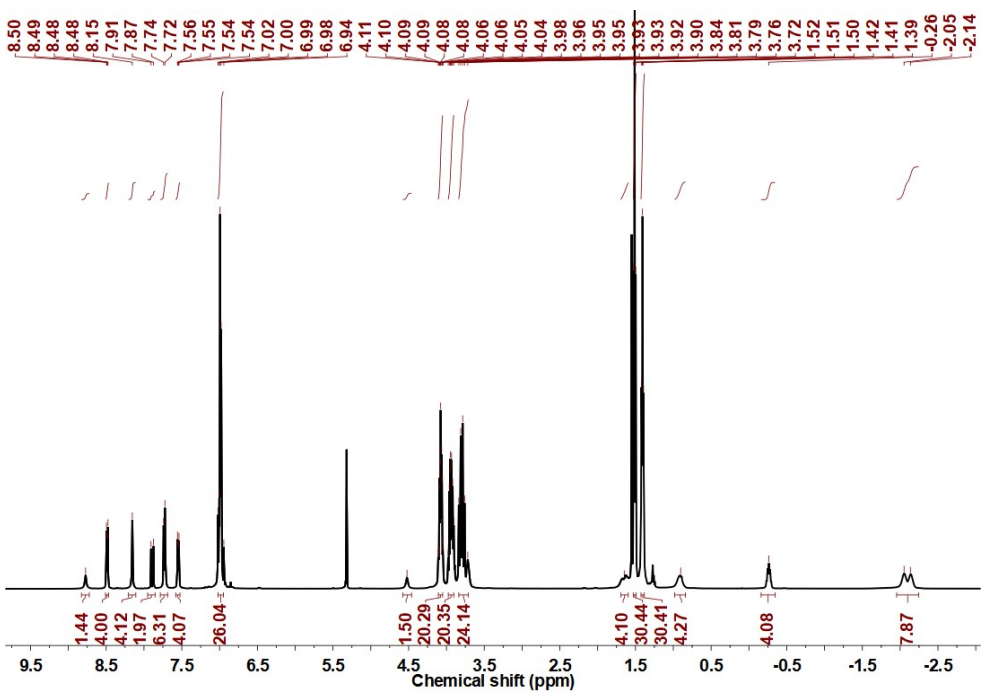

Figure S38. ^{1}H NMR spectrum (500 MHz, CD_2Cl_2, 298K) of the [3]rotaxane **R**.

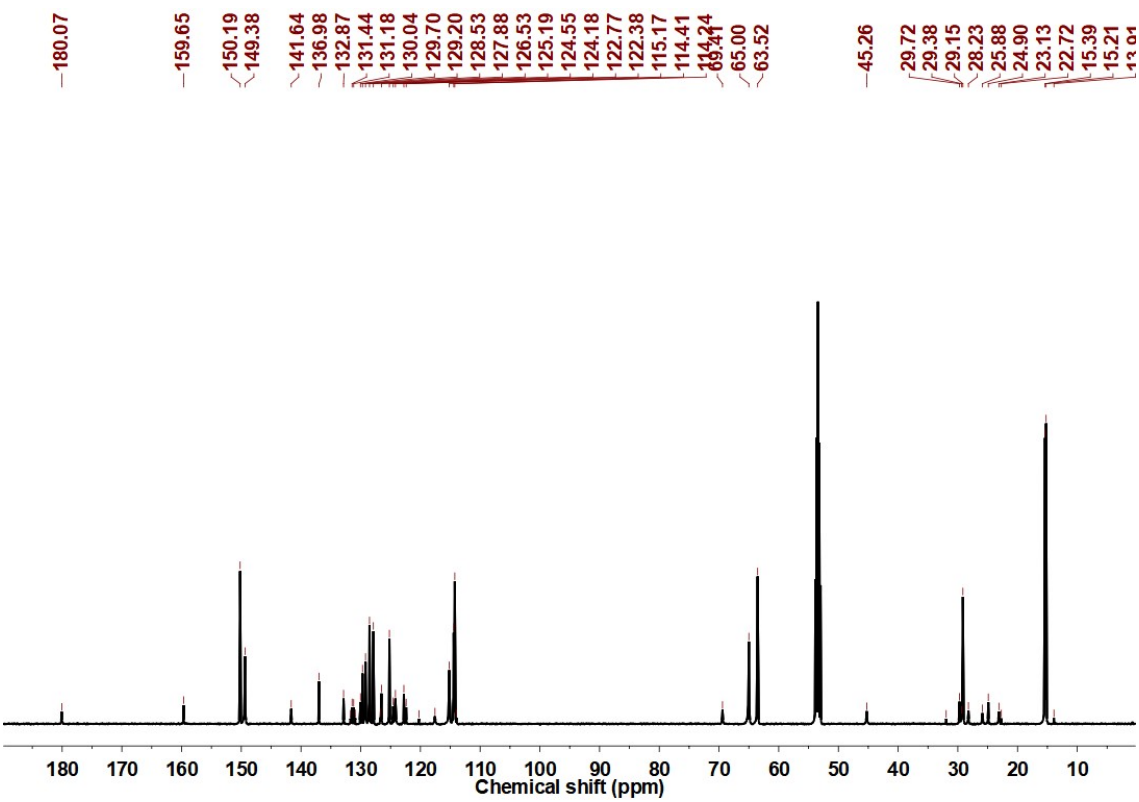

Figure S39. ^{13}C NMR spectrum (125 MHz, CD_2Cl_2, 298 K) of the [3]rotaxane **R**.

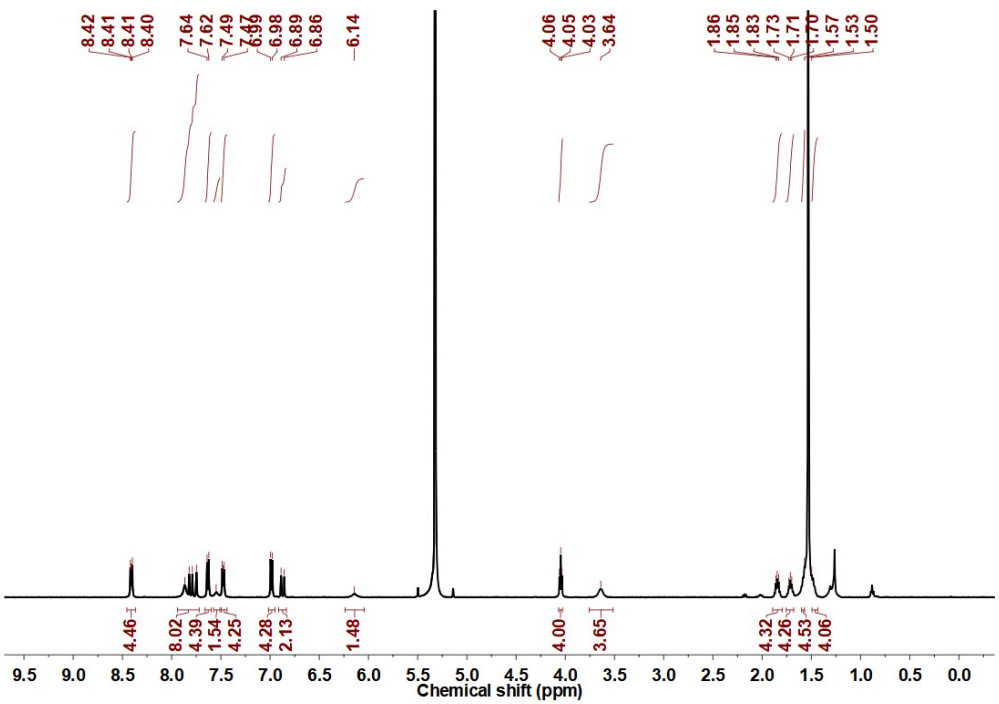

Figure S40. ^{1}H NMR spectrum (500 MHz, CD_2Cl_2, 298K) of the linear molecular axle **A**.

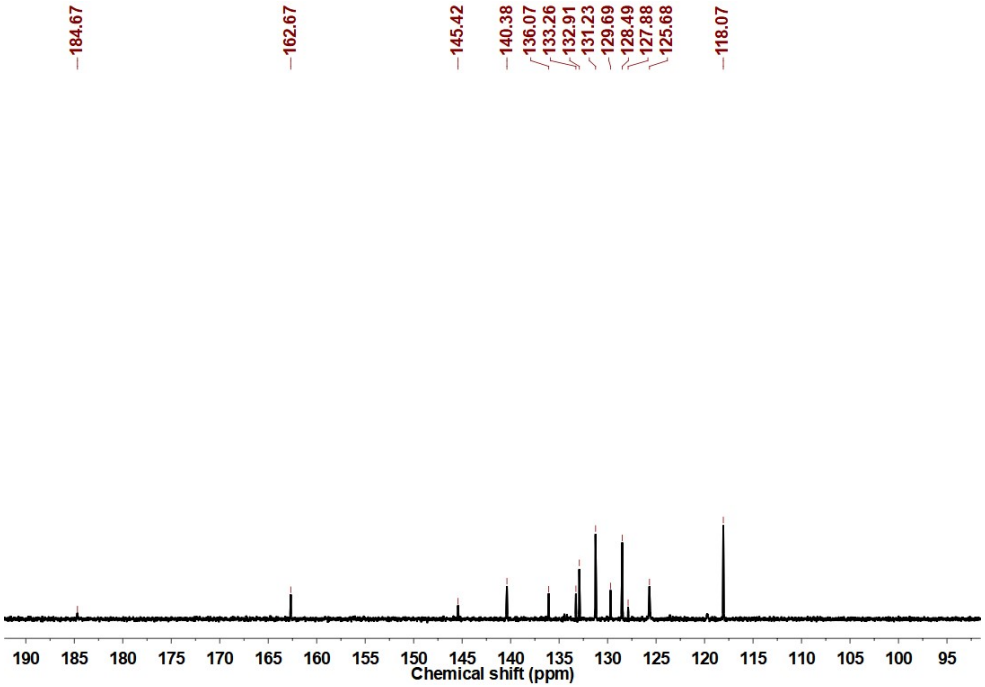

Figure 41. ^{13}C NMR spectrum (125 MHz, CD_2Cl_2, 298 K) of the linear molecular axle **A**.

7. References.

1. Li-Jun Chen and Hai-Bo Yang, Construction of Stimuli-Responsive Functional Materials via Hierarchical Self-Assembly Involving Coordination Interactions, *Acc. Chem. Res*. **2018**, *51*, 2699.

2. Wei Wang, Li-Jun Chen, Xu-Qing Wang, Bin Sun, Xiaopeng Li, Yanyan Zhang, Jiameng Shi, Yihua Yu, Li Zhang, Minghua Liu, Hai-Bo Yang, Organometallic rotaxane dendrimers with fourth-generation mechanically interlocked branches, *Proc. Natl. Acad. Sci. U.S.A*. **2015**, *112*, 5597.

3. Xu-Qing Wang, Wei-Jian Li, Wei Wang, Jin Wen, Ying Zhang, Hongwei Tan, Hai-Bo Yang, Construction of Type III-C rotaxane-branched dendrimers and their anion-induced dimension modulation feature, *J. Am. Chem. Soc*. **2019**, *141*, 13923.

4. He-Ye Zhou, Qian-Shou Zong, Ying Han and Chuan-Feng Chen, Recent advances in higher order rotaxane architectures, Chem. Commun., **2020**, *56*, 9916.Shengyi Dong, Jiayin Yuan and Feihe Huang, A pillar[5]arene/imidazolium [2]rotaxane: solvent- and thermo-driven molecular motions and supramolecular gel formation, *Chem. Sci*., **2014**, 5, 247.